International Journal of Precision Engineering and Manufacturing (2021) 22:271–285
https://doi.org/10.1007/s12541-020-00405-w

Online ISSN 2005-4602
Print ISSN 2234-7593

REGULAR PAPER

Verification of Rotordynamic Design Using 1/5 Scaled Model Rotor of 270 MW-Class Gas Turbine Center-Tied Rotor

Yeong-Chun Kim[1] · Sang-Sup Han[1] · Young-Cheol Kim[2]

Received: 8 August 2019 / Revised: 26 March 2020 / Accepted: 12 August 2020 / Published online: 4 January 2021

Abstract

Gas turbine power generation is relatively minor in terms of pollutant emissions, such as nitrogen oxides or sulfur oxides, as compared to thermal power generation using coal or petroleum. This is because of the use of liquefied natural gas, known as an eco-friendly power generation solution. Large gas turbines used for power generation are suitable for the power load demanded by modern society, which fluctuates very much with respect to power consumption because it takes only about 10–20 min to reach the entire output from the start-up. A large gas turbine used for power generation is a rotating machine that features a high degree of difficulty in mechanical design due to its fast start-up characteristics, structural complexity, and high operating temperature, while also emphasizing stability. Customers are demanding operational reliability as a prerequisite before evaluating the performance of a gas turbine. It is very important to design and verify the rotor dynamics sufficiently and accurately from the design stage prior to fabrication in light of that it is very difficult to change the rotor dynamics characteristics once the design is completed and finished. Many researchers are trying to improve the design completeness, but the researches that actually design and verify the power generation gas turbine are limited only to a few manufacturers with the original technology, so there is little verification of actual gas turbine. In this paper, rotor dynamics analysis and verification of a 270 MW class DGT-300H gas turbine rotor newly developed by DHI. To verify the center tie-rod type rotor design of a large gas turbine for power generation, which was conceptually designed using in-house design tools, a 1/5 scaled model was designed by applying the dynamic scaling law. In order to verify the suitability of the applied tie-rod design, the characteristics of the variation of the natural frequency with the variation of the pre-tightening force were tested in order to confirm the dynamic proper pre-tightening force. The design of the scaled model rotor was created, the model was designed and fabricated, and the natural frequencies were analyzed and tested to confirm the validity of the design method and the suitability of the analysis results. After the design of the large gas turbine rotor for 270 MW class power generation, the natural frequencies of the rotor before the blade installation were analyzed and the suitability of the design was verified by implementing a vibration test of the rotor before blade installation.

Keywords Large gas turbine rotor · Center-tied rotor · Hirth coupling · Verification of gas turbine rotordynamics · Pre-tightening force · Scaled model rotor

✉ Yeong-Chun Kim
yeongchun.kim@doosan.com

Sang-Sup Han
sangsup.han@doosan.com

Young-Cheol Kim
kyc@kimm.re.kr

[1] Gas Turbine BU, Doosan Heavy Industries, 22, DoosanVolvo-ro, Seongsan-gu, Changwon, Gyeongnam, Korea

[2] Mechanical Systems Safety Research Division, Korea Institute of Machinery and Materials, 156 Gajeongbuk-Ro, Yuseong-Gu, Daejeon 34103, Korea

1 Introduction

Gas turbine power generation is relatively minor in terms of pollutant emissions, such as nitrogen oxides or sulfur oxides, as compared to thermal power generation using coal or petroleum. This is because of the use of liquefied natural gas, known as an eco-friendly power generation solution. Large gas turbines used for power generation are suitable for the power load demanded by modern society, which fluctuates very much with respect to power consumption because it takes only about 10–20 min to reach the entire output from the start-up [1–3].

Recently, the use of renewable energy sources found in wind and photovoltaic power have increased very rapidly in response to the demand for global eco-friendly power generation. Although such wind and solar power generation systems do not use fossil fuels nor generate pollutants, they have a limit of intermittency because the electric power produced depends on nature (wind, sun) [2–10].

For this reason, renewable power generation should use an energy storage system to compensate for fluctuations in output. However, except for small-scale power generation, most renewable power generation systems tend to be constructed in large-scale complexes to improve the usability of the installation sites and the efficiency of maintenance. Since the output fluctuation of a large-scale renewable power generation system is very big, it is difficult to cope with a general energy storage system such as a battery. Therefore, a large-capacity energy backup system that compensates for output volatility is inevitably required for a large-scale renewable power generation. Gas turbine power generation is also increasing in value as a large-capacity energy backup system [2, 7, 8].

The large gas turbine used for power generation is a rotating machine that requires a high degree of difficulty in mechanical design due to its fast start-up characteristics, structural complexity, and high operating temperature, as it emphasizes stability [9, 10].

In fact, despite the progress of many design and manufacturing technologies, power generation turbines are causing many problems during operation. Most of the major problems that arise are design-related, with more than half of the high-speed rotating machines experiencing a high vibration during the critical speed at which they operate. However, with these large high-speed rotating machines, unscheduled facility shutdowns occur due to the vibration of the rotor-bearing system which account for more than 50% of the total number of high-speed rotating machine accidents. A lot of time is required to solve the problem (sometimes taking more than 100 weeks) [11, 12].

Gas turbines for large-scale power generation have a very complicated structure, such as a flexible hollow shaft, a conical rotating structure, and a thin plate-shaped casing to realize the advantages of being lightweight and highly efficient, reliable, durable, and safe. This means that the system can reach the rated operating speed only when it passes several critical speeds. Therefore, it is necessary to predict and design precise dynamic behavior through rotor dynamics analysis to ensure reliability and stability. Hence, the rotor dynamics and structural dynamics designs of the gas turbine are what make it successful [13, 14].

Also, users require operational reliability (stability) as a precondition before evaluating the performance (efficiency) and price of the gas turbine. After the design is completed and the fabrication is finished, it is very difficult to make big changes to the rotor-dynamic characteristics. Therefore, it is very important to design and verify the rotor-dynamic characteristics sufficiently and accurately starting at the design stage before they are manufactured.

For precise rotor dynamic analysis, calculation of accuracy should be increased, and the following should be checked: rotor element partition, taper and step modeling, mass concentration, stiffness effect on the disk and coupling, the variation of material properties in regard to temperature, dynamic characteristics of bearing, and stiffness effect on the bearing support structure.

To secure the stability of operation, accurate prediction of the critical speed is very important in the separation margin design, and it is important to ensure the consistency between the analysis results and the test results. Many researchers are working to improve the design of gas turbines, but the researches that design and verify gas turbines for power generation are limited by manufacturers with some of the original technologies, so there are few verification results for actual gas turbines.

In this paper, we have designed a scaled model of a rotor, which is conceptually designed for the verification of the rotor dynamic analysis method of the DGT-300H gas turbine rotor (Fig. 1) which is under development at DHI, by applying the dynamic scaling law. The results were verified through an impact test. Based on these results, the rotor design of the gas turbine being developed is completed, and the rotor dynamic design of the manufactured rotor is verified by the impact test.

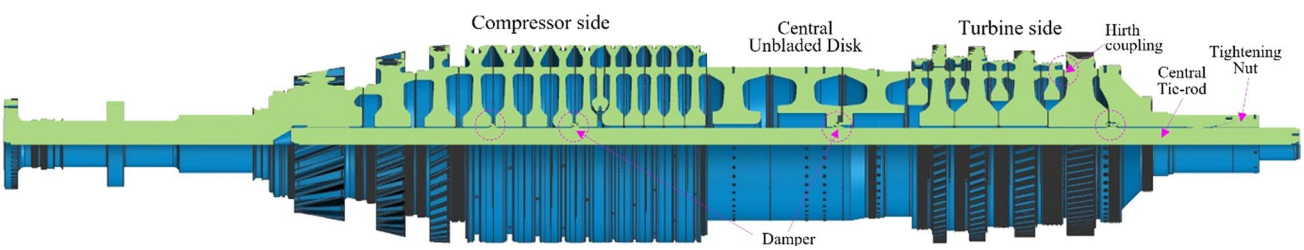

Fig. 1 Cutaway view of DGT-300H gas turbine rotor

2 Design of Rotor

2.1 Background

The turbine rotor is composed of a rotating shaft, a rotating disk, and a rotating blade, and has a complicated structure in which a coupling relationship is considered in each of these characteristics. To satisfy the high power output condition, it is necessary to accommodate a large amount of flow at high rotational speed, which is disadvantageous in terms of dynamic stability compared to other rotating machines of similar size [14]. Therefore, it is necessary to perform rotordynamic analysis on the rotor from the initial stage of design, to predict the vibration response at the critical speed and the operation speed at which the resonance occurs, and to determine the stability.

There are three main ways to complete the entire rotor assembly, such as the compressor of a gas turbine or each stage disc of a turbine [15].

(1) Welded elastic bridges,
(2) Sliding Hirth serrations with a central tie bolt,
(3) Tight fits with multiple mid-span tie bolts

The large gas turbines include sliding Hirth serrations with a central tie bolt system, an original equipment manufacturer in Europe of Siemens, and tight fits with multiple mid-span tie bolts system, an original equipment manufacturer GE of U.S. and an original equipment manufacturer MHPS of Japan.

Generally, assembled rotors should be designed so that the concentricity and parallelism in the joint coupling are kept within a few microns to avoid vibration. The joint coupling increases the coupling diameter to provide the required bending stiffness and strength. The mechanical coupling should generally not cause any slippage in the joint or make the slip very uniform along the circumferential direction as in the case of radial serration like Hirth. This means the friction coefficient should be consistent and low. The temperature of bolts and disks, elasticity in a joint coupling should be adjusted to maintain pre-tension in all situations [15, 16].

The Hirth coupling method used for inter-disc coupling increases the torque transfer capability significantly compared to the plane coupling, and especially when an impact torque due to a generator fault occurs. Also, it is easy to form an internal cooling path through a gap between gears, and thermal load in a transient state due to rapid heat transfer of the disk is reduced It is effective [16, 17]. Hirth coupling has a self-centering function and has a radial degree of freedom, which is advantageous in relieving stress due to thermal expansion. Since the center tie is not a torque transfer by face to face friction, it is known that the level of tie rod pre-stress does not need to exceed 50% of the yield stress. The method using the center tie rod is advantageous in that the assembly process is simple since it is assembled with one rod and the cyclic load due to static deflection is small [16].

The subject of study in this paper is center tie-rod built-up gas turbine rotor (Fig. 1) adopted by DGT-300H developed by DHI (Doosan Heavy Industries). The basic structure of the DGT-300H rotor, which is the subject of the study, consists of a compressor with 13 stages and a turbine with 4 stages, and CUD (Central Unblade Disk) consists of three stages. These compressor disks, torque disks, and turbine disks are shown in Fig. 1, all are connected by Hirth Coupling. The center tie-rod has a structure that is connected to the center of the disk from the compressor to the turbine at one time and supports the disk and the tie-rod in contact with the disk by placing a damper in the middle.

2.2 Design of Rotor

Figure 2 shows the shape of the Hirth coupling, which is the inter-disc coupling structure of the rotor to be analyzed [17]. The design of the center tie-rod built-up GT rotor with this coupling determines the pre-tightening force of the tie-rod to maintain the integrity of the gas turbine rotor, and the dimension of the tie-rod. Then, the equivalent stiffness diameter is selected by performing the bending stiffness analysis of the joint coupling based on the designed shape of the contact area, and the rotor dynamic analysis is performed based on the equivalent stiffness diameter [18].

$$F_T = T/R_m \tag{1}$$

$$F_A = F_T \tan(\beta - \rho) \tag{2}$$

where T external torque, F_T total tangential force, F_A total axial force, β tooth angle, R_m mean radius of the tooth $(R_i+R_o)/2$, ρ angle of friction

$$\begin{aligned}\sigma_P &= F_A/A \\ &= 4F_A/\pi(D^2 - d^2)\end{aligned} \tag{3}$$

$$\sigma_T = \frac{T(\tan\beta - \mu)}{R_m A_z(1 + \mu\tan\beta)} \tag{4}$$

$$\sigma_B = \frac{32MD}{\pi(D^4 - d^4)} \tag{5}$$

where σ_P nominal equivalent pre-tightening stress, σ_T separating stress due to torque, σ_B separating stress due to bending, A_Z effective tooth contact area, μ friction coefficient

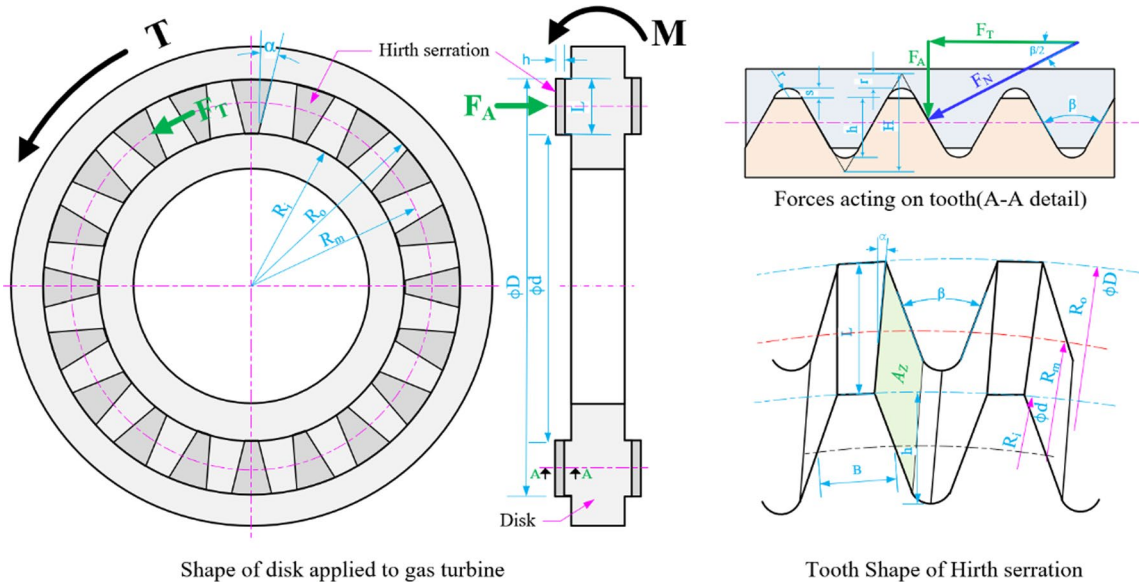

Fig. 2 Shape of GT disk with hirth serration

tan ρ, A nominal contact area, M bending moment, D outer diameter of the teeth, d inner diameter of the teeth

$$\gamma_B = \frac{\sigma_B}{\sigma_P} \tag{6}$$

$$\gamma_T = \frac{\sigma_T}{\sigma_P} \tag{7}$$

where γ_B non-dimensional bending stiffness coefficient, γ_T non-dimensional torsional stiffness coefficient.

The rotor must maintain its integrity by the bending moment due to the weight of the rotor and the bending moment due to blade loss. Therefore, the pre-tightening force is determined so that the non-dimensional bending stiffness coefficient γ_B is smaller than 1. In particular, when the bending moment is due to the rotor weight, it is recommended that the non-dimensional bending stiffness coefficient be designed to be around 0.1. The pre-tightening force is determined so that the non-dimensional torsional stiffness coefficient γ_T is less than 1.0 to maintain the integrity even under the rated torque condition and maintain the integrity under the transient torque conditions of the generator fault condition.

2.2.1 Pre-tightening Force Determination

The pre-tightening force of the tie-rod bolt, which determines the integrity of the gas turbine rotor, is determined by the following three criteria: [16]

(1) Criterion considering bending moment. The pre-tightening force of the tie-rod bolt is determined to endure separating moment of bearing-supported rotor weight. It is significantly applied when one of the blades is lost while operation, especially one of the fourth-stage blades of a turbine or one of the first-stage blades of compressor [19].
(2) Criterion considering transmission torque. Integrity should be maintained while disk in operation with maximum torque, considering. Moreover, integrity should be maintained even in the condition of impact torque occurring, such as generator fault.
(3) Criterion considering natural frequency. Integrity should be verified with natural frequency convergence condition according to the pre-tightening force. Mainly can be found in the modal test of the rotor.

2.2.2 Stress Criterion for Tie-Rod Structural Design

In general, the pre-tightening stress due to the pre-tightening force on the designed tie rod is assembled to 50% of the yield stress which is 0.2% tensile condition of rod length (directional strain 0.2%). Normally, the stress is changed to 45–60% of the yield stress in the start-up period, and when the steady-state operation is reached, 50% of the yield stress is maintained (Fig. 3) [16]. Therefore, it should be operated while maintaining the stress within the yield stress range at the centrifugal force and temperature conditions in the start-up period.

Table 1 Parameters of tie bolt rotor of gas turbine

Gas turbine	GE9FA	M701F	V94.3	DGT-300H
Rotor weight (tons)	78	89		69
Power (MW)	255	240	273	270
No. of tie-bolts (EA)	**15** (multi)	**12** (multi)	**1** (single)	**1** (single)
Material	NiCrMoV	IN718	26Cr2MoV115	26NiCrMoV145
Yield stress (MPa)	710	1124	822	835
Pre-tightening force (N)	2.36×10^6	2.73×10^6	2.45×10^7	2.56×10^7
Pre-stress/yield stress	**0.5**	**0.533**	**0.484**	**0.52**
Tie-bolt diameter (mm)	92	76.2	280	280
γ_B (σ_B/σ_P)	**0.09**	**0.11**	**0.10**	**0.13**
γ_T (σ_T/σ_P)	**0.48**	**0.42**	**0.76**	**0.84**

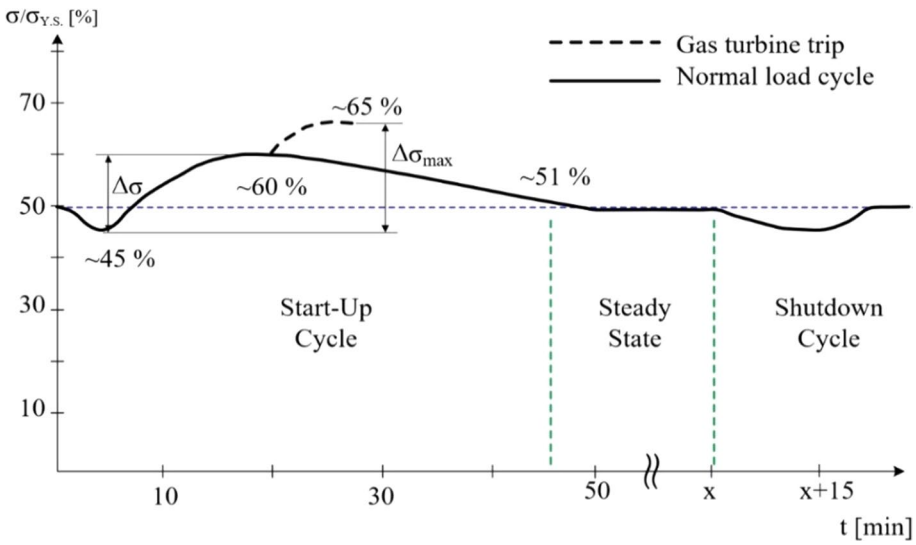

Fig. 3 Mechanical and thermal load cycle of a rotor tie-rod [16]

Table 1 compares the design parameters of major manufacturers. As expected, the ratio of pre-tightening stress/yield stress is 50%, γ_B is 0.1 and γ_T is 0.8 (center tie-rod γ_T is 0.80, multi tie-rod γ_T is 0.46). DHI's DGT-300H is similarly designed with γ_B 0.13 and γ_T 0.84, which are not significantly different from those of other manufacturers.

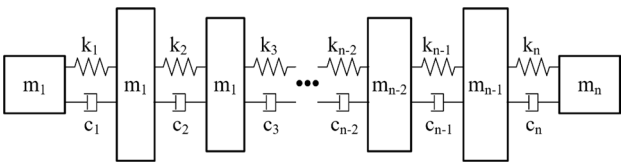

Fig. 4 Dynamic modeling of rotor

3 Analysis and Experiment of Scaled Rotor

3.1 Scaled Model Rotor Design

To verify the dynamics design of the DGT-300H rotor, a one-fifth size model rotor is designed. The reason for using the scaled model is to find the representation of the scaling factor and law for static, dynamic similitude between full-size system and scaled model, and to expect physical characteristics (e.g., natural frequency, displacement, velocity, force) of the full-size system [13].

The rotor system of the turbine is shown in Fig. 4, and the equation of motion can be written as Eq. (8) [20–22].

$$[M]\{\ddot{u}\} + [C]\{\dot{u}\}+[K]\{u\} = \{F(t)\} \tag{8}$$

where $\{u\}$, $\{\dot{u}\}$ and $\{\ddot{u}\}$ are displacement vector, velocity and acceleration vectors, $[M]$, $[C]$ and $[K]$ are the overall mass, damping and stiffness matrices, $\{F(t)\}$ external force vector of the rotor-bearing system.

3.1.1 Scaling Factors Between the Full-Sized Rotor and Scaled Model

The dynamic similarity of the rotor system is derived from Eqs. (8) to (13) derived by Wu [23–26] For a vibration

system with damping, the equation of motion can be written as [24].

$$m_{ii}^{(q)}\frac{d^2\eta_i^{(q)}}{dt_i^{(q)^2}}+2m_{ii}^{(q)}\zeta_i^{(q)}\omega_i^{(q)}\frac{d\eta_i^{(q)}}{dt_i^{(q)}}+m_{ii}^{(q)}\omega_i^{(q)^2}\eta_i^{(q)}=f_i^{(q)}(t^{(q)})\quad(q=s,F) \tag{9}$$

where m_{ii} generalized mass, ζ_i generalized damping ratio, η_i generalized displacement, ω_i ith natural frequency, $f_i(t)$ generalized force

$$\left(\frac{\lambda_{im}\lambda_{i\eta}}{\lambda_t^2\lambda_{if}}\right)m_{ii}^{(\mathrm{F})}\frac{d^2\eta_i^{(\mathrm{F})}}{dt_i^{(\mathrm{F})^2}}+\left(\frac{\lambda_{im}\lambda_{i\zeta}\lambda_{i\omega}\lambda_{i\eta}}{\lambda_t\lambda_{if}}\right)2m_{ii}^{(\mathrm{F})}\zeta_i^{(\mathrm{F})}\omega_i^{(\mathrm{F})}\frac{d\eta_i^{(\mathrm{F})}}{dt_i^{(\mathrm{F})}}+\left(\frac{\lambda_{im}\lambda_{i\omega}^2\lambda_{i\eta}}{\lambda_{if}}\right)m_{ii}^{(\mathrm{F})}\omega_i^{(\mathrm{F})^2}\eta_i^{(\mathrm{F})}=f_i^{(\mathrm{F})}(t^{(\mathrm{F})}) \tag{10}$$

Equation (10) is the equation of motion of the entire rotor system that vibrates to the ith mode obtained based on the equation of motion and related scale parameters of scale model rotor. Equations (9) and (10) should be equivalent, so the following relation holds [23].

Table 2 Physical parameters of scaled rotor

Description	Scale law	1/5 scale model
Diameter of bearing journal	λ_η	100 mm
Max. outer diameter of disk	λ_η	350 mm
Total length of disks	λ_η	1438 mm
Type of disk to disk coupling		Hirth-serration
No. of disk (Comp./CUD/TBN)	1	13/3/4
Diameter of center tie-rod	λ_η	64 mm
Length of center tie-rod	λ_η	1540 mm
Total length of rotor	λ_η	2927 mm
Total weight of rotor	λ_η^3	642 kgf
Material of shaft and disks		SCM440

$$\frac{\lambda_{im}\lambda_{i\eta}}{\lambda_t^2\lambda_{if}}=\frac{\lambda_{im}\lambda_{i\zeta}\lambda_{i\omega}\lambda_{i\eta}}{\lambda_t\lambda_{if}}=\frac{\lambda_{im}\lambda_{i\omega}^2\lambda_{i\eta}}{\lambda_{if}}=1 \tag{11}$$

$$\lambda_t=\lambda_\eta,\quad \lambda_\omega=1/\lambda_\eta,\quad \lambda_m=\lambda_\eta^3,\quad \lambda_\zeta=1,\quad \lambda_f=\lambda_\eta^2 \tag{12}$$

$$\lambda_k=\lambda_m\lambda_\omega^2=\lambda_\eta^3(1/\lambda_\eta^2)=\lambda_\eta,\quad \lambda_I=\lambda_{I_P}=\lambda_\eta^5 \tag{13}$$

where λ_η scaling factor of length, λ_m scaling factor of the generalized mass λ_I, λ_{I_P} scaling factor of mass moment of inertia of disk (I_p, I_D).

The requirement of similitude between the full-size model and scale model is equivalent to Eq. (11), so scaling factor can be determined as Eqs. (12) and (13) [23]. The design of scale model ($\lambda_\eta = 1/5$) is based on scaling law as Table 1, determined as Table 2 considering experimental conditions. Figure 5 is a design of a one-fifth scale model.

The pre-tightening force of tie-rod which maintains the integrity of the scale-model rotor is determined, and the size of tie-rod is selected based on the pre-tightening force. Based on the designed shape of the disk contact area, the maximum bending moment due to the rotor weight in joint coupling is about 2556 N-m. Based on this, the coupling force required to maintain the coupling state of a disk calculated with a non-dimensional bending stiffness coefficient of 0.1, is about 725 kN. The pre-tightening force of scale-model tie-rod is 73.9 tons, and stress on the tie-rod was designed at a level of 24% compared to the yield stress

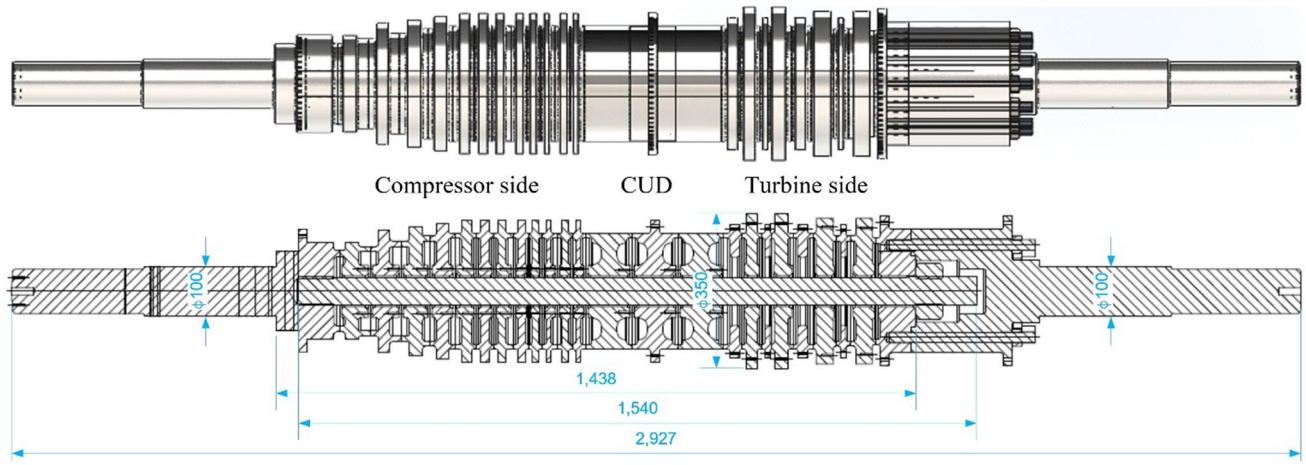

Fig. 5 1/5 Scaled model rotor

of the rod. Moreover, the maximum bending moment due to the rotor weight in joint coupling based on the designed shape of the disk contact area is 600 N-m.

3.2 Experimental and Analysis Results

As shown in Fig. 5, the scale model was designed and fabricated with a total length of 2.9 m and a total weight of 653.4 kgf, and the number of disks was the same as the actual number of disks, 13 stages for compressors, 3 stages for CUD and 4 stages for turbines. The specifications of the materials used in the construction are as shown in Table 3.

While assembling the scale-model rotor, disks are stacked by order on the stacking jig, and the tie-rod is assembled. Following the temporary assembly, the nut was fastened after applying the target pre-tightening force to the tie-rod using the hydraulic system.

Experiments of the scaled rotor were conducted based on a free–free condition, the natural frequency was found from the frequency response function (FRF) through the impact test, changing the pre-tightening force from 5.2 to 120 tons (Fig. 6). The equipment used in the experiments is as shown in Table 4.

Rotordynamic analysis of the scale model was made using the DYNAMICS R4, considering contact stiffness effect based on GW theory, applying 45° rule (or 30° rule) in rapid section change, using equivalent stiffness coefficient of tie-bolts [27–32].

In the impact test of the scaled model rotor, since the experiment must be performed while changing the pre-tightening force applied to the tie-rod, the tie-rod is disassembled and assembled repeatedly using a hydraulic system. The modal analysis results and vibration test results according to the pre-tightening force changes (5.2, 10.3, 20.7, 31.0, 41.3, 51.6, 62.0, 73.9, 87.8 and 120.0 tons) were compared (Table 5, Fig. 7).

The FRF of the impact test is shown in Figs. 8, 9, 10, 11, 12 and 13. As shown in the Frequency response function, it can be seen that the natural frequency increases as the pre-tightening force increases. That is, the 1st natural frequency is 120–130.2 Hz, the 2nd natural frequency is 126.3–170.2 Hz, and the 3rd natural frequency is 206.7–217.2 Hz.

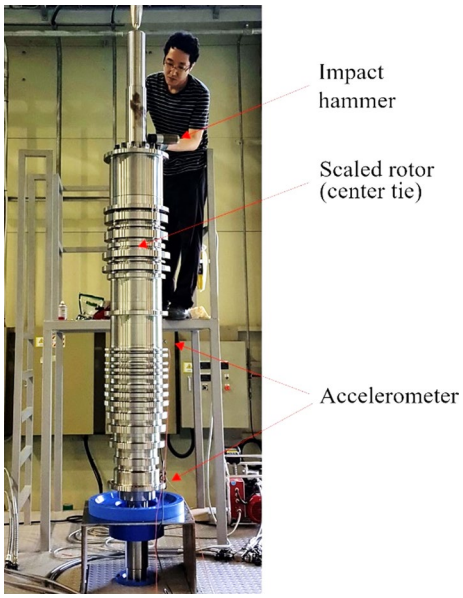

Fig. 6 Impact test of scaled model rotor

As a result of the analysis, the 1st natural frequency is 121.5–131.2 Hz, the 2nd natural frequency is 150.1–168.9 Hz, and the 3rd natural frequency is 210.3–216.3 Hz.

Also, as the pre-tightening force increases, the natural frequency of the rotor gradually converges, and since the contact surface is large, the pre-tightening force effect appears more clearly in the first to third natural frequencies.

If the pre-tightening force is above the threshold, it can be seen that the dynamic characteristics are similar to those of an integral rotor. Therefore, to prevent the change of the tightening force due to the thermal effect caused by operation mode and to prevent the change of the rotor dynamic characteristics due to the change, the pre-tightening stress/yield stress ratio was increased to 24%. It is reasonable to increase the pre-tightening force by 50% to 120 tons (1.2E+6N).

As shown in the results of Fig. 7 and Table 5, the analysis results are not significantly different from the Measured results, so the analysis method is considered to be sufficiently reliable. If the pre-tightening stress/yield stress ratio is 0.3, i.e., the pre-tightening force is only about 100 tons,

Table 3 Material properties of scaled rotor

Material	SCM440(AISI4140H)
Density	7850 kg/m^3
Young's modulus	205 GPa
Poisson's ratio	0.29
Yield strength	685 MPa
Tensile strength	883 MPa

Table 4 Experimental equipment

No.	Equipment	Model no.
1	Multi-ch. FFT analyzer	M+P Smart Analyzer
2	Impact hammer	PCB 5802A
3	Amplifier	NI 9234+NI 9184
4	Accelerometer	Dytran 3035B

Table 5 Comparison of the natural frequency of calculated and experimental results

Pre-tightening (tons)	1st Natural frequency (Hz)			2nd Natural frequency (Hz)			3rd Natural frequency (Hz)		
	Calc.	Meas.	Error (%)	Calc.	Meas.	Error (%)	Calc.	Meas.	Error (%)
5.2	121.5	120.0	1.3	150.1	126.3	18.9	210.3	206.7	1.7
10.3	125.4	120.5	4.1	151.5	140.9	7.5	213.1	213.4	0.2
20.7	127.8	124.4	2.7	153.5	147.3	4.2	214.6	215.9	0.6
31.0	128.8	125.3	2.8	155.3	150.3	3.3	215.2	215.8	0.3
41.3	129.5	126.1	2.7	156.9	153.8	2.0	215.5	215.8	0.1
51.6	129.9	127.0	2.3	158.5	155.8	1.7	215.7	216.7	0.5
62.0	130.3	127.0	2.6	160.1	158.0	1.3	215.9	215.8	0.1
73.9	130.6	128.3	1.8	162.0	160.6	0.9	216.0	215.9	0.0
87.8	130.9	129.3	1.2	164.1	163.4	0.4	216.2	216.1	0.1
120.0	131.2	130.2	0.8	168.9	170.2	0.7	216.3	217.2	0.4

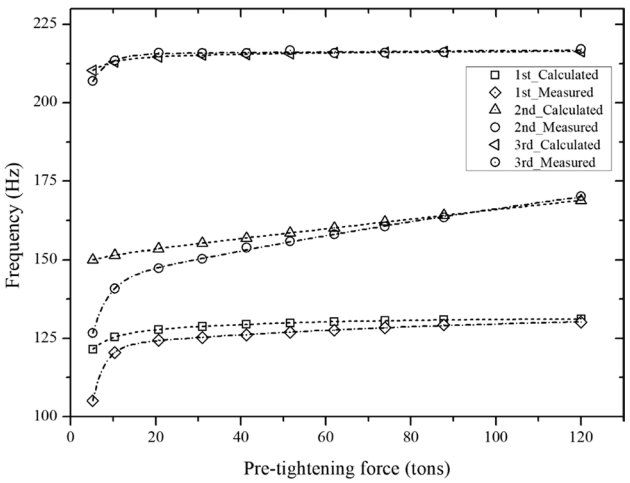

Fig. 7 Comparison of calculated and measured natural frequencies

the error is less than 1%. If the pre-tightening stress/yield stress ratio is about 0.5, i.e., the pre-tightening force is about 154 tons as in the design standard, the error level is expected to be about 0.5%.

If the pre-tightening force is about 154 tons, the pre-tightening stress due to the pre-tightening force is about 50% of the yield stress. This result is consistent with Janssen's [16]. Therefore, it is confirmed that the condition of convergence of the natural frequency according to the pre-tightening force satisfies the pre-tightening stress/yield stress ratio ≈ 0.5 conditions as the selection criterion considering natural frequency.

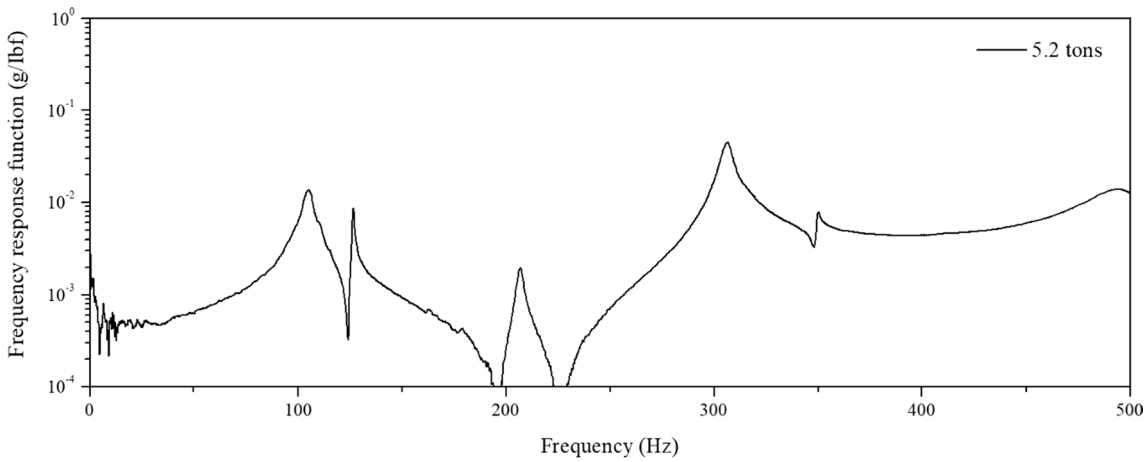

Fig. 8 Frequency response function at 5.2 tons pre-tightening force

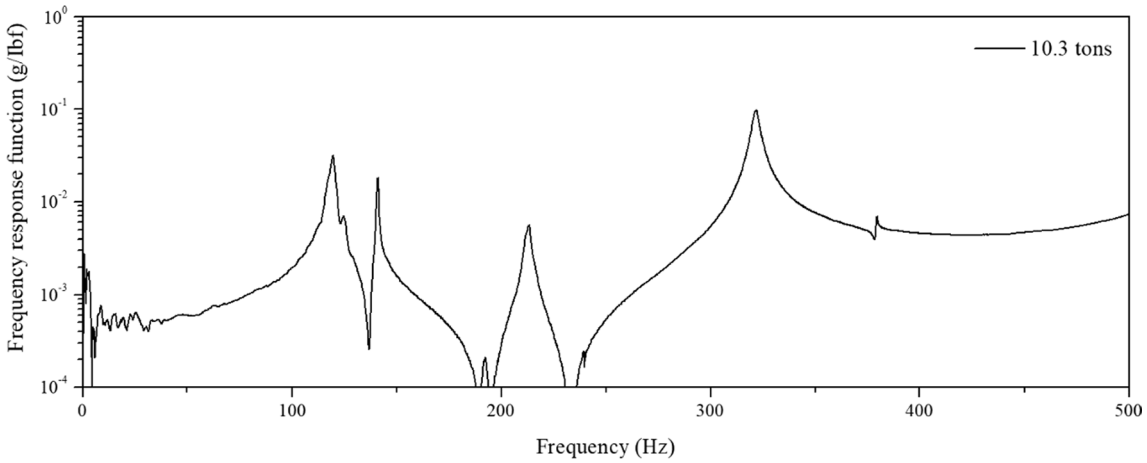

Fig. 9 Frequency response function at 10.3 tons pre-tightening force

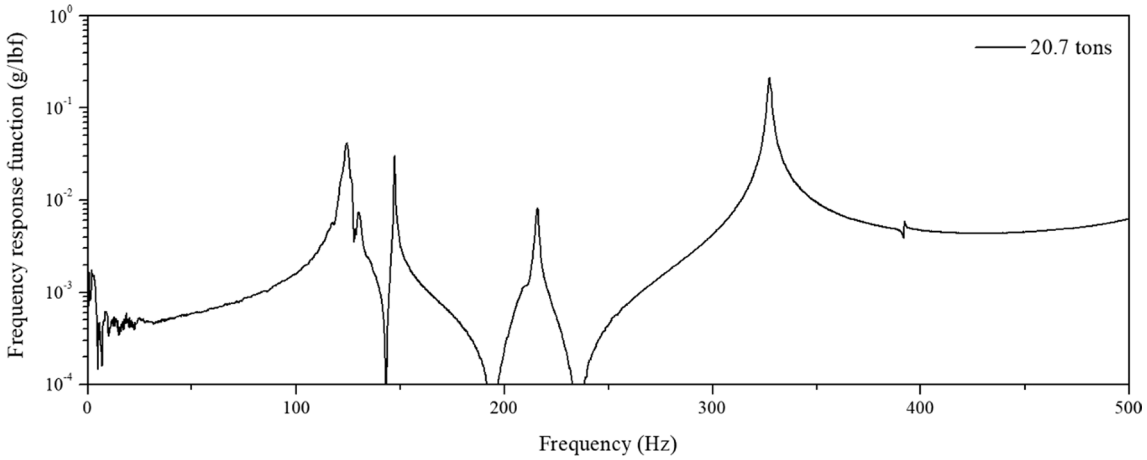

Fig. 10 Frequency response function at 20.7 tons pre-tightening force

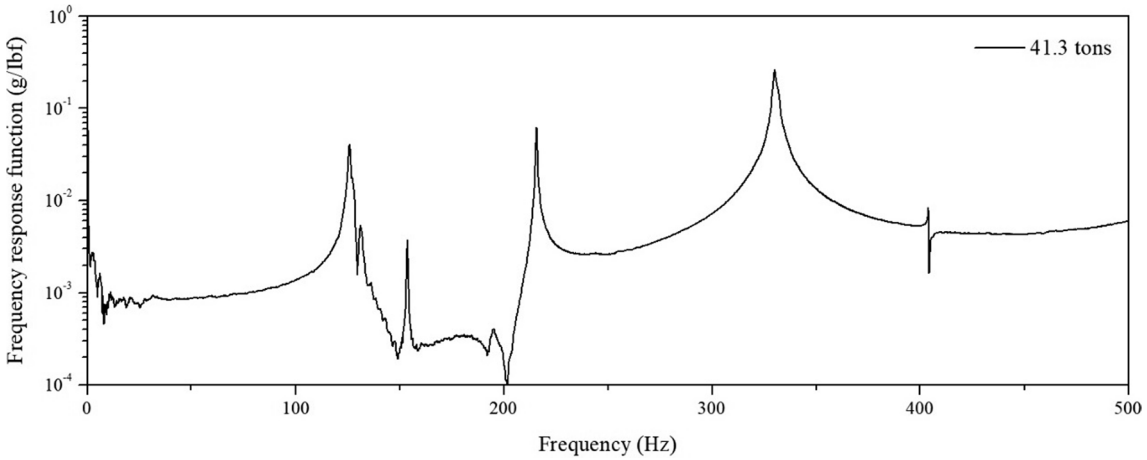

Fig. 11 Frequency response function at 41.3 tons pre-tightening force

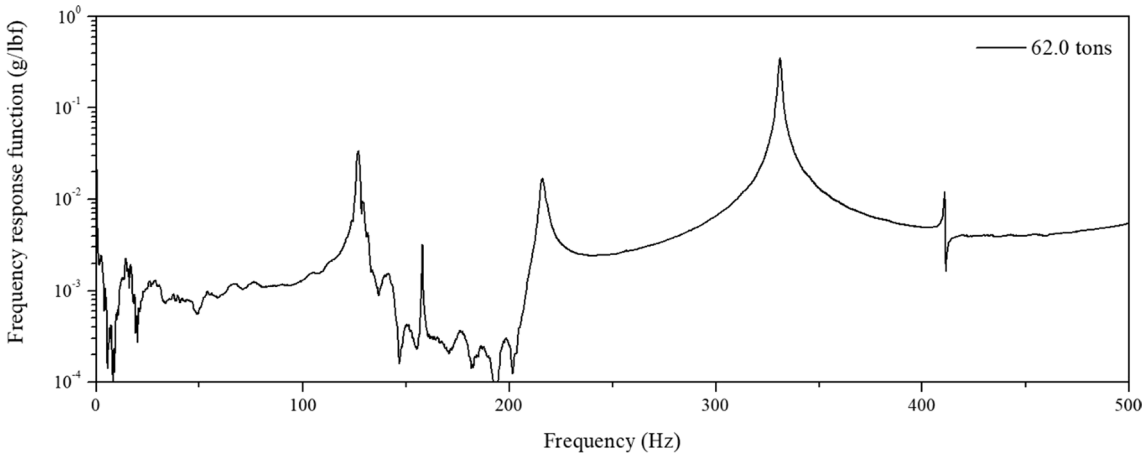

Fig. 12 Frequency response function at 62.0 tons pre-tightening force

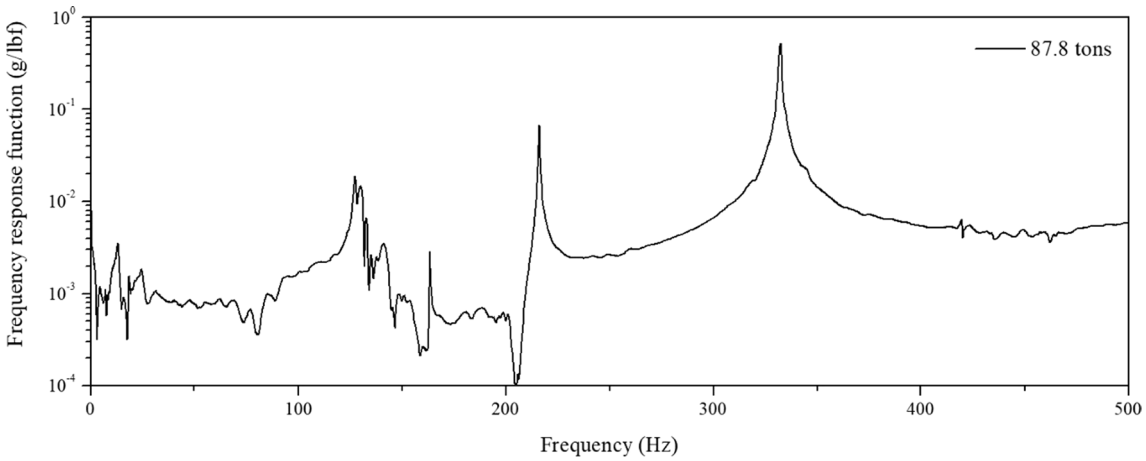

Fig. 13 Frequency response function at 87.8 tons pre-tightening force

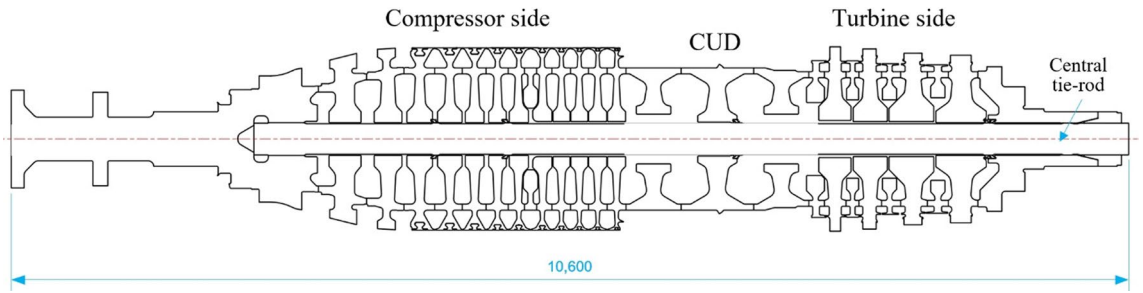

Fig. 14 Full-scale unbladed real rotor

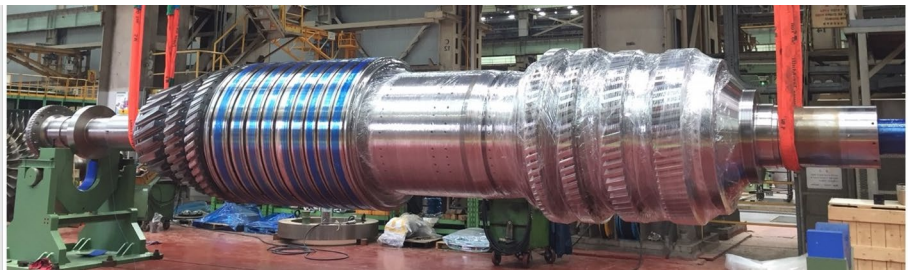

Fig. 15 Impact test of unbladed real rotor, free–free condition

Table 6 Material properties of central tie-rod

Material	26NiCrMoV145
Density	7850 kg/m^3
Young's modulus	211.4 GPa
Poisson's ratio	0.29
Yield strength	835 MPa
Tensile strength	1005 MPa

4 Analysis and Experiment of Full-Scale Rotor

4.1 Experimental and Analysis Results (Full-Scale Unbladed Rotor)

The DGT-300H S1 rotor, which is self-designed and manufactured by DHI, is shown in Fig. 14. As shown in Fig. 15, the overall length was designed and fabricated at 10.6 m, and the rotor was made of an assembly with 13 stages of the compressor, 3 stages of CUD, 4 stages of turbine, total 20 disks. The test object is a rotor in which the disk is assembled and the blades are not assembled. Table 6 shows the specifications of the materials used in the analysis of the actual rotor. The materials used in the actual fabrication were different from those of Table 6 in consideration of the stress conditions at each position by centrifugal force, temperature, and compressive force.

As shown in Fig. 16, the rotor was assembled vertically in a special assembly facility, and the pre-tightening force applied was 26 MN, which is 50% of yield stress, based on data verified by a scale model.

The rotordynamic analysis for the full-scale rotor uses DYNAMICS R4, which is a commercially available tool, as used for the scaled rotor model analysis, and the proven method is applied to the scaled model rotor analysis. In other words, the contact stiffness effect based on the GW theory was considered. In the case of a rapid section change, the 45° rule (or 30° rule) was applied and the equivalent stiffness coefficient of the Tie-bolts was used Respectively. The results of the analysis were 45.9 Hz for 1st natural frequency, 81.3 Hz for 2nd natural frequency, 130.1 Hz for 3rd natural frequency as shown in Fig. 17.

Fig. 16 Photo of rotor assembly

For natural frequency verification, the experiment is shown in Fig. 15, the rotor was suspended and subjected to an impact test using an impact hammer under a free–free condition. From the frequency response function (FRF) measured through the impact test, The natural frequency was confirmed. The test results are shown in Fig. 18, the 1st natural frequency is 45.7 Hz, the 2nd natural frequency is 79.5 Hz, and the 3rd natural frequency is 139.0 Hz.

As shown in Table 7, Comparing the analysis results with the experimental results, the errors in the first to third modes are 0.3%, 2.3%, and 0.8%, respectively. The second-order mode error is relatively large because the

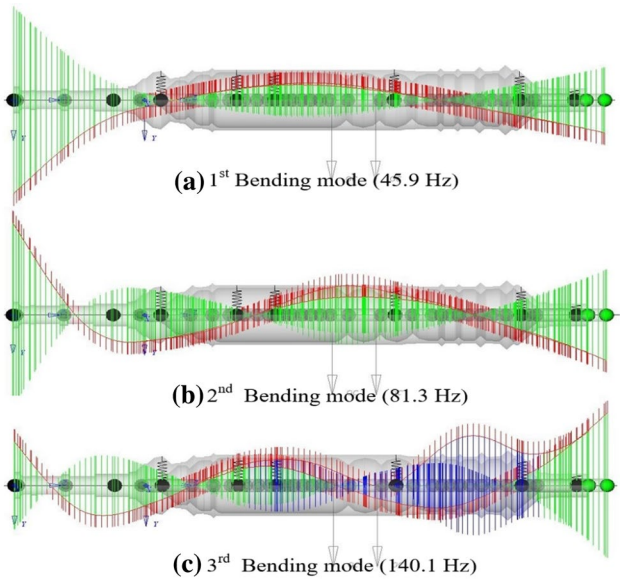

Fig. 17 The result of modal analysis of full-scale rotor

properties of the materials used at the inflection point of the second mode are different from those of the material used for the analysis. In other words, the material to be used is selected in consideration of long-periods operation under the conditions of centrifugal force, temperature, and compressive force. Since the rotor is composed of many disks and the temperature distribution differs depending on the operation of the disk, a material that can withstand thermal stress and life is selected for each disk [33–35].

Figure 19 compares a scaled model rotor with a full scale rotor. It may be difficult to directly compare the dynamic characteristics between the two rotors by looking at the figure. In practice, the main target of dynamic comparisons is the tie-rod with the disks being combined.

5 Conclusion

The gas turbine is rotating machinery with a high emphasis on operational stability, and despite advances in design and manufacturing technology, it causes many problems during operation. Therefore, customers are demanding operation stability as a precondition for the gas turbine. It is very important to accurately design and verify the turbine from the design stage since it is hard to change the rotordynamic characteristics of the gas turbine after design and fabrication are completed.

The problem addressed in this paper is to secure operation stability in a rotor that uses a large number of disks assembled with a center tie-rod. To solve this problem, a rotor model is used to verify the rotor dynamics and analysis method in advance, and the actual rotor is designed and manufactured based on the verified data, the natural frequency is measured by the impact test, to confirm the design and fabrication quality by comparing the results of the validated analysis.

The following conclusions were obtained through the analysis and experiments of the scaled model rotor and the actual full-scale rotor:

(1) The natural frequency changes according to the pressing force to be assembled with the center tie rod, and the natural frequency converges as the pressing force increases.

Table 7 The result of modal analysis and test of the full-scale rotor

Order	Analysis (Hz)	Test (Hz)	Difference (%)
1st	45.9	45.8	0.3
2nd	91.3	79.5	2.3
3rd	140.1	139.0	0.8

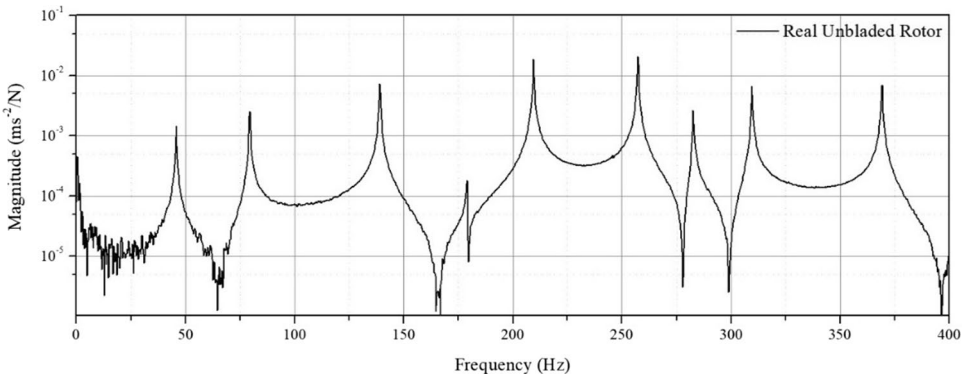

Fig. 18 Frequency response function of unbladed real rotor

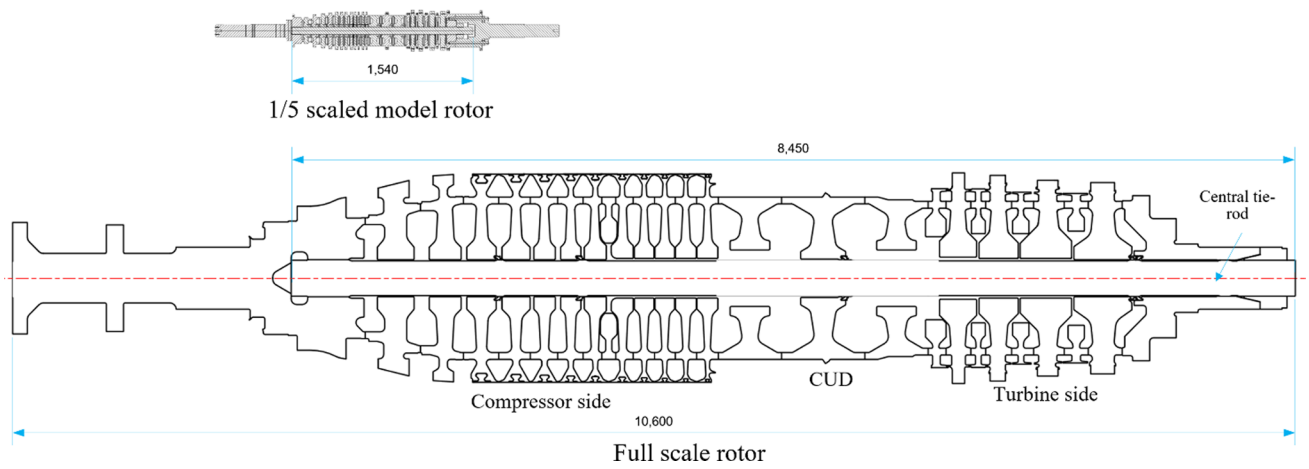

Fig. 19 Size comparison with scaled model rotor and full scale rotor

(2) The non-dimensional bending stiffness coefficient (γ_B) due to the weight of the rotor at the joint coupling is designed to be about 0.1 based on the contact geometry of the designed disk.
(3) Since the pre-tightening stress/yield stress ratio reaches 30%, natural frequency converges, and in 50%, it is consistent with the test results within 0.5%, so it is considered reasonable to compress to a level of 50%.
(4) Considering the contact stiffness effect in the analysis of the rotor and applying a 45° rule (or 30° rule) where there is a sudden change in section and applying the equivalent stiffness coefficient of the tie-bolts, It can be expected that a sufficient level of analysis accuracy can be expected.
(5) To improve the accuracy of the actual rotor analysis, different materials are used depending on the environment (temperature, stress, and service life) of each disk, so the actual mechanical properties of the material to be used must be applied.
(6) Since the analysis and experiment results of a scale model applying the scaling law of a gas turbine rotor show sufficient consistency with the actual rotor analysis and experiment results, the pre-assessment through a scale model was found to be sufficiently useful.

Acknowledgements This research was supported by the Korea Institute of Energy Technology Evaluation and Planning (KETEP) funded by the Korea government (Ministry of Trade, Industry, and Energy (MOTIE) (No. 2013101010170A).

References

1. Gülen, S. C. (2019). Gas turbines for electric power generation. *Gas Turbines for Electric Power Generation*. https://doi.org/10.1017/9781108241625.
2. Pieper, C., & Rubel, H. (2012). Electricity storage making large-scale adoption of wind and solar energies a reality. *Balanced Growth*. https://doi.org/10.1007/978-3-642-24653-1_11.
3. Kost, C., Shammugam, S., Julch, V., Nguyen, H., & Schelegl, T. (2018). Levelized cost of electricity renewable energy technologies. *Fraunhofer Institute for Solar Energy Systems ISE*, 1–42.
4. U.S. EIA. (2019). Annual energy outlook 2019 with projections to 2050. *44*(8), 1–64.
5. Gonzalez-Salazar, M. A., Kirsten, T., & Prchlik, L. (2018). Review of the operational flexibility and emissions of gas- and coal-fired power plants in a future with growing renewables. *Renewable and Sustainable Energy Reviews, 82*(July 2017), 1497–1513. https://doi.org/10.1016/j.rser.2017.05.278.
6. Lee, A., Zinaman, O., & Logan, J. (2012). *Opportunities for synergy between natural gas and renewable energy in the electric power and transportation sectors*. Technical Report NREL (December).
7. Dickel, R. (2018). *The role of natural gas, renewables and energy efficiency in decarbonisation in Germany: The need to complement renewables by decarbonized gas to meet the Paris targets*. OIES Paper: NG 129. https://doi.org/10.23946/2500-0764-2017-2-2-70-76.
8. National Academy of Sciences and Engineering (acatech), German National Academy of Sciences Leopoldina, & Union of the German Academies of Sciences and Humanities. (2016). *Flexibility concepts for the German power supply in 2050, Ensuring stability in the age of renewable energies. Series on Science-Based Policy Advice*.
9. Appavou, F., Brown, A., Epp, B., Gibb, D., Kondev, B., McCrone, A., Murdock, H. E., Musolino, E., Ranalder, L., Sawin, J. L., Seyboth, K., & Jonathan Skeen, F. S. (2019). *Renewbles in Cities - 2019 Global Status Report*. REN21 Secretariat. Retrieved from https://wedocs.unep.org/bitstream/handle/20.500.11822/28496/REN2019.pdf?sequence=1&isAllowed=y%0Ahttp://www.ren21.net/cities/wp-content/uploads/2019/05/REC-GSR-Low-Res.pdf.

10. Society, A. P. (2010). *Integrating renewable electricity on the grid a report by the APS Panel on Public Affairs*. In The APS Panel on Public Affairs (POPA) (p. 40). American Physical Society.
11. Cook, C. P. (1985). Shop vs. field corrections to equipment. In *Proceedings of the 14th turbomachinery symposium*. Texas A&M University. Turbomachinery Laboratories.
12. Bloch, H. P. (1998). *Improving machinery reliability, practical machinery management for process plants* (Vol. 1). Houston, TX: Gulf Professional Publishing.
13. Lee, A. S. (1998). Rotor dynamic design supervision for the reliability of the rotating machinery. *Noise and Vibration, 8*(5), 775–783.
14. Korea Institute of Machinery and Materials. (1998). *Conceptual design of a heavy duty gas turbine engine for power generation*. Ministry of Science & Technology of KOREA. Retrieved from http://www.riss.kr/link?id=M11723632.
15. Endres, W. (1992). Rotor design for large industrial gas turbines. In *ASME 1992 international gas turbine and aeroengine congress and exposition* (p. V005T14A033-V005T14A033). Citeseer.
16. Janssen, M. J., & Joyce, J. S. (2015). 35-year old splined-disc rotor design for large gas turbines (p. V005T14A060). ASME International. https://doi.org/10.1115/96-gt-523.
17. Croccolo, D., De Agostinis, M., Fini, S., Olmi, G., Robusto, F., & Vincenzi, N. (2018). On Hirth ring couplings: design principles including the effect of friction. *Actuators, 7*(4), 79. https://doi.org/10.3390/act7040079.
18. Archer, R. R., Crandall, S. H., Dahl, N. C., Lardner, T. J., & Sivakumar, M. S. (2012). *An introduction to mechanics of solids*. New York: Tata McGraw-Hill Education.
19. Jiang, X.-J., Zhang, Y.-Y., & Yuan, S.-X. (2012). Analysis of the contact stresses in curvic couplings of gas turbine in a blade-off event. *Strength of Materials, 44*(5), 539–550.
20. Vance, J., Fouad, Y., & Zeidan, B. G. M. (2010). *Machinery vibration and rotordynamics*. Hoboken: Wiley.
21. Lee, C.-W. (1993). *Vibration analysis of rotors* (Vol. 21). Berlin: Springer.
22. Kim, Y.-C., & Kim, K.-W. (2006). Influence of lamination pressure upon the stiffness of laminated rotor. *JSME International Journal Series C, 49*(2), 426–431. https://doi.org/10.1299/jsmec.49.426.
23. Wu, J. J. (2007). Prediction of lateral vibration characteristics of a full-size rotor-bearing system by using those of its scale models. *Finite Elements in Analysis and Design, 43*(10), 803–816. https://doi.org/10.1016/j.finel.2007.05.001.
24. Bathe, K.-J. (2014). *Finite element procedures* (2nd Ed.). Englewood Cliffs, NJ: Klaus-Jurgen Bathe. Retrieved from http://www.amazon.com/Finite-Element-Procedures-Part-1-2/dp/0133014584.
25. Rastogi, G., Moin, K., & Abbas, S. M. (2015). Dimensional analysis and development of similitude rules for dynamic structural models. *International Journal of Emerging Technology and Advanced Engineering, 5*(3), 68–72.
26. Coutinho, C. J. P. (2017). *Structural reduced scale models based on similitude theory*. University of Porto (FEUP).
27. Sanderson, N., & Kitching, R. (1978). Flexibility of shafts with abrupt changes of section. *International Journal of Mechanical Sciences, 20,* 189–199.
28. Choi, S. P. (2003). *Vibration analysis and optimum design of large steam turbine rotor*. Pukyung National University, Busan. Retrieved from http://www.riss.kr/link?id=T9823237.
29. Liu, Y., Yuan, Q., & Zhou, Z. (2015). Contact status analysis of rod-fastened rotors with hirth coupling in gas turbines. In *ASME turbo expo 2015: Turbine technical conference and exposition* (pp. GT2015-42816). American Society of Mechanical Engineers.
30. Gao, J., Yuan, Q., Li, P., Feng, Z., Zhang, H., & Lv, Z. (2012). Effects of bending moments and pretightening forces on the flexural stiffness of contact interfaces in rod-fastened rotors. In *Proceedings of ASME turbo expo 2012* (pp. GT2012-68221). American Society of Mechanical Engineers.
31. Yuan, Q., Gao, R., Feng, Z., & Wang, J. (2008). Analysis of dynamic characteristics of gas turbine rotor considering contact effects and pre-tightening force. In *ASME Turbo Expo 2008: Power for land, sea, and air* (pp. 983–988). American Society of Mechanical Engineers. https://doi.org/10.1115/gt2008-50396.
32. Liu, X., Yuan, Q., Liu, Y., & Gao, J. (2014). Analysis of the stiffness of hirth couplings in rod-fastened rotors based on experimental modal parameter identification. In *Proceedings of ASME turbo expo 2014: Turbine technical conference and exposition* (p. V07AT31A027). ASME International. https://doi.org/10.1115/gt2014-26448.
33. Benini, E. (Ed.). (2011). *Advances in gas turbine technology*. London: InTech. https://doi.org/10.5772/664.
34. Singh, K. (2014). Advanced materials for land based gas turbines. *Transactions of the Indian Institute of Metals*. https://doi.org/10.1007/s12666-014-0398-3.
35. Singh, P., Kaurase, K. P., & Soni, G. (2015). *Study of materials used in gas turbine engine and swirler in combustion chamber* (Vol. 1). Retrieved from www.ijariie.com.

Yeong-Chun Kim received his B.S., M.S. degree in Mechanical Engineering from the Kumoh National University of Technology in 1986 and 1991, respectively. He received his Ph.D. degrees in Mechanical Engineering from the Korea Advanced Institute of Science & Technology(KAIST), Korea, in 2003. He is currently a Principal Research Engineer in Doosan Heavy Industries, Korea. His research interests include Rotordynamic design of Steam & Gas turbine, bearing system design, and vibration diagnosis of Turbomachinery.

Sang-Sup Han received his B.S. degree in Mechanical Engineering from Halla University in 2004. He received his M.S. degree in Mechanical Engineering at Seoul National University, Korea, in 2007. He is currently a lead research engineer in Doosan Heavy Industries & Construction, Korea. His research interests include Turbine Rotordynamics and Power Transmission Design.

Young-Cheol Kim received his B.S., M.S. degree in Mechanical Engineering from the Pusan National University in 1990 and 1993, respectively. He received his Ph.D. degrees in Mechanical Engineering from the Korea Advanced Institute of Science & Technology(KAIST), Korea, in 2008. He is currently a Principal Research Engineer in Korea Institute of Machinery & Materials(KIMM), Korea. His research interests include rotordynamics, tribology, and energy harvesting.